Mineral. Deposita 31, 394–406 (1996)

MINERALIUM DEPOSITA

Fluid inclusion evidence for the physicochemical conditions of sulfide deposition in the Olympias carbonate-hosted Pb-Zn(Au, Ag) sulfide ore deposit, E. Chalkidiki peninsula, N. Greece

S.P. Kilias[1], S.I. Kalogeropoulos[2], J. Konnerup-Madsen[3]

[1] Institute of Geology and Mineral Exploration (IGME), 1, Fragon Str., 546 26 Thessaloniki, Greece
[2] Rusvar Holdings BV, 4, Nikis Str., 105 62 Athens, Greece
[3] University of Copenhagen, Geological Institute, Oster Voldgade 10, DK-1350 Copenhagen K, Denmark

Received: 22 April 1994/Accepted: 30 January 1996

Abstract. The Olympias Pb-Zn(Au, Ag) sulfide ore deposit, E. Chalkidiki, N. Greece, is hosted by marbles of the polymetamorphic Kerdilia Formation of Paleozoic or older age. The geologic environment of the ore also comprises biotite-hornblende gneisses and amphibolites intruded by Tertiary pegmatite-aplite dikes, lamprophyre dikes, the 30-Ma Stratoni granodiorite, and porphyritic stocks. Only limited parts of the deposit display shear folding and brecciation; most of it is undeformed. Microthermometry of fluid inclusions in gangue syn-ore quartz indicates three types of primary and pseudosecondary inclusions: (1) H_2O-rich, 1–18 wt. % NaCl equivalent, <3.6 mol % CO_2; (2) H_2O-CO_2 inclusions, <4 wt. % NaCl equivalent, with variable CO_2 contents, coexisting in both undeformed and deformed ore; (3) aqueous, high-salinity (28–32 wt. % NaCl equivalent) inclusions found only in undeformed ore. Type 2 inclusions are differentiated into two sub-types: (2a) relatively constant CO_2 content in the narrow range of 8–15 mol % and homogenization to the liquid phase; (2b) variable CO_2 content between 18 and 50 mol % and homogenization to the vapor phase. Type 1 and 2b inclusions are consistent with trapping of two fluids by unmixing of a high-temperature, saline, aqueous, CO_2-bearing fluid of possible magmatic origin, probably trapped in type 2a inclusions. Fluid unmixing and concomitant ore mineralization took place at temperatures of 350 ± 30 °C and fluctuating pressures of less than 500 bar, for both undeformed and deformed ores. The wide salinity range of type 1 inclusions probably represents a complex effect of salinity increase, due to fluid unmixing and volatile loss, and dilution, due to mixing with low-salinity meteoric waters. High solute enrichment of the residual liquid, due to extreme volatile loss during unmixing, may account for high salinity type 3 inclusions. The Olympias fluid inclusion salinity-temperature gradients bear similarities to analogous gradients related to Pb-Zn ores formed in "granite"-hosted, low-T distal-skarn, skarn-free carbonate-replacement and epithermal environments.

The Olympias Pb-Zn(Au, Ag) sulfide ore deposit is hosted by marbles of the amphibolite facies Kerdilia Formation, and is located 5 km west of the town of Olympias, in the E. Chalkidiki peninsula, northern Greece (Fig. 1). Current mining activity in the area including carbonate-hosted Pb-Zn(Au, Ag) orebodies of Olympias, Madem Lakos, and Mavres Petres (Fig. 1) produces about 550 000 tons/y with 4% Pb, 4% Zn, 0.15% Cu, 110 ppm Ag and 1.5 ppm Au.

The origin of the Olympias, and Madem Lakos ores (Fig. 1) is subject to controversy. Nicolaou and Kokonis (1980) supported a metasomatic replacement origin for the ores at the Olympias deposit based on geological evidence and ore textures Mantzos (1989) and Nebel et al. (1991) suggested a premetamorphic syngenetic origin for the Olympias and Madem Lakos ores which were subsequently regionally metamorphosed and later reworked by Tertiary hydrothermal activity related to igneous rocks in the area. In a comprehensive study of the Olympias deposit, Kalogeropoulos et al. (1989) described undeformed and deformed ore varieties, and presented field, mineralogical, geochemical, and stable and radiogenic isotopic data supportive of a single event of epigenetic-replacement origin related to Tertiary magmatic activity. In the latter study, a brief summary of fluid inclusion data was included based on preliminary data of Kilias and Kalogeropoulos (1989). The debate about the Madem Lakos polymetallic ores (epigenetic vs. remobilized syngenetic) is included in Kalogeropoulos et al. (1989), Nebel et al. (1991), Gilg et al. (1992) and Nebel et al. (1992). On the basis of geochronological data Gilg and Frei (1994) favored an epigenetic origin of the ores and a genetic relationship to the emplacement of Tertiary porphyritic stocks in the area of eastern Chalkidiki.

This study deals with microthermometry of syn-ore gangue material from undeformed and deformed Olympias ores in an attempt to solve this debate.

Correspondence to: S.P. Kilias

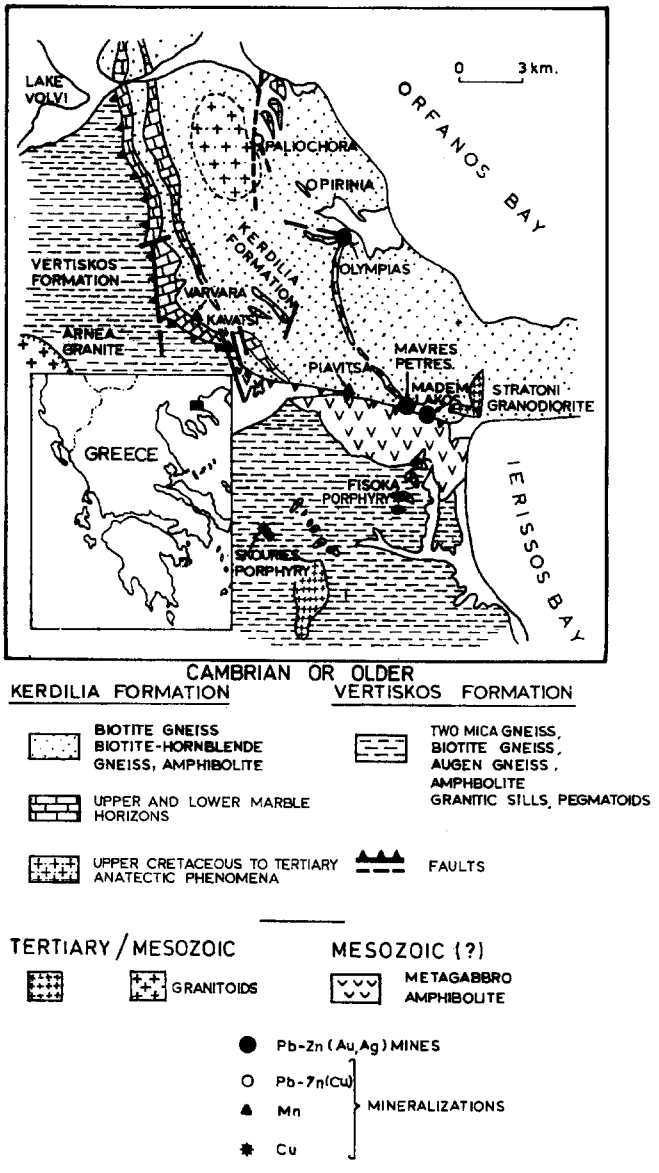

Fig. 1. Simplified geologic map of Eastern Chalkidiki showing the location of the Olympias mine (modified from Kockel et al. 1977)

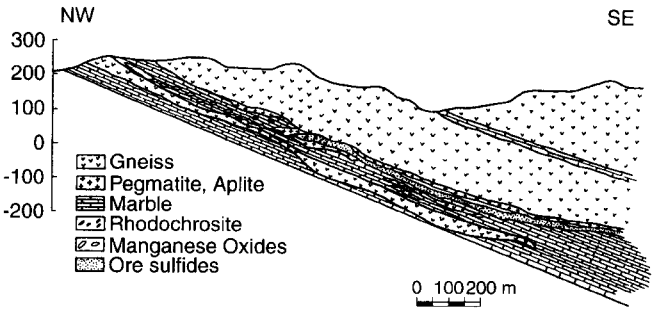

Fig. 2. Longitudinal geologic section of the Olympias deposit (Nicolaou and Kokonis 1980)

Olympias deposit

The geology of the Olympias mine, and the regional geologic setting of the ores, are described in detail in Nicolaou and Kokonis (1980) and Kalogeropoulos et al. (1989), and only a short review is given here.

The Olympias Pb-Zn(Au, Ag) sulfide deposit is hosted by marbles of the Paleozoic or older Kerdilia Formation. The host rocks of the ores consist predominantly of marbles, biotite-hornblende gneisses of either sedimentary or igneous origin, and amphibolites of primarily igneous origin. These rocks have been regionally deformed and metamorphosed under amphibolite facies conditions of 5 to 9 kbar pressure, and 550° to 650 °C temperature. This event is interpreted to have lasted until the Tertiary, culminated by the intrusion of pegmatite-aplite dikes, lamprophyre dikes, the 30-Ma Stratoni granodiorite, and granodioritic to quartz dioritic (Fisoka-24–25 Ma) and syenitic (Skouries-20 Ma) porphyries (Fig. 1). This stage of anatexis and calc-alkaline magmatism is also characterized by contact metamorphism to the greenschist facies.

The deposit is generally stratabound (manto) or fracture controlled; it strikes NNW for 1500 m, dips 30 to 35° SW to a depth of at least 300 m, and has an average thickness of 12 m. It develops within a lower marble horizon along the contact with an overlying unit of biotite gneiss (Fig. 2). The contacts between the ore and host marble are sharp, concordant or discordant to the foliation. In all cases, the host marble is characterized by a reaction front zone up to 0.5 m wide along the contact with the ore. This hydrothermal alteration halo is characterized by a decrease in the amount of graphite, higher quartz contents and recrystallized carbonate. These mineralogical changes are accompanied by enrichment in SiO_2, FeO, MgO, MnO, Ag, Pb, Zn and S, and a depletion in CaO (Kalogeropoulos et al. 1987).

The ore occurs in undeformed and deformed varieties. The former predominates and is present in several forms such as cavity- and fracture-filling, banded or disseminated. The deformed ore is limited in quantity and occurs banded or in veins exhibiting shear folding and brecciation.

The main minerals present in both undeformed and deformed ore varieties are pyrite, sphalerite, galena, and arsenopyrite, whereas the principal gangue mineralogy consists of quartz, calcite, and rhodochrosite.

Undeformed ore minerals occur in coarse idiomorphic crystals exhibiting growth zoning (pyrite, arsenopyrite), in polycrystalline aggregates, including crystals with linear polysynthetic twinning or wide chromatic zoning (sphalerite), and coarse-grained crystals (galena). Recrystallization in pyrite, brittle deformation in arsenopyrite, as well as pyrite, deformation twinning and mylonitization in sphalerite, and bend cleavage, kink banding and translation gliding in galena are characteristic textures of deformed ore minerals. Deformed and undeformed sphalerites exhibit similar chromatic and chemical zoning, and growth zoning is also shown by deformed arsenopyrite.

Fluid inclusion study

Ore samples were collected from the −92 m, −102 m, −112 m, −122 m and −132 m levels at the Olympias mine for fluid inclusion microthermometry. Microthermometric measurements were conducted on carefully selected fluid inclusions in chips of doubly polished sections of 100 to 200 μm thickness, using a Leitz microscope equipped with a Chaixmeca heating and cooling stage (Poty et al. 1976) at the Institute of Petrology, University of Copenhagen, Denmark. The stage was calibrated in the temperature range of −100° to 600 °C using various melting point standards. The uncertainty in the temperature measurements of the phase changes described is ±0.5 °C. Heating and freezing runs were performed on gangue quartz belonging to both the undeformed (20 samples) and deformed (8 samples) varieties of the mineralization. Calculation of fluid properties from observed microthermometric data on individual inclusions was done with the use of the FLINCOR (Brown 1989) program.

Host quartz

Quartz occurs as a gangue mineral in the following associations: (1) in cavity filling ore, in concentric bands of rhodochrosite and sulfides; (2) in banded ore, in deci to deca-metric scale bands with sulfides; (3) in vein-type ore filling faults and fractures in the host rock; (4) as a minor constituent of polymictic ore breccias, and it has also been observed in the form of tight isoclinally folded bands in folded banded ore (Kalogeropoulos et al. 1989).

Quartz hosting the studied fluid inclusions is always intimately intergrown with ore sulfides, and appears to be in textural and physicochemical equilibrium with them. The quartz crystals on which the fluid inclusion study was conducted were: (1) euhedral to subhedral, clear or zoned, and typically conforming to the shape of coexisting sulfides (undeformed ore) (Fig. 3A); (2) anhedral or elongated showing strained extinction, healed brittle microfractures both intragranular and crosscutting, irregular or curved boundaries against coexisting sulfides (Fig. 3B), or sutured margins (deformed ore). Clear quartz grain domains with uniform optical extinction and isolated from transgranular fracture planes were sampled for fluid inclusion study. Recrystallized quartz grains either by hydrothermal fluids or other stages of recrystallization associated with undeformed and deformed ore, respectively (Kalogeropoulos et al. 1989), were avoided.

Types of fluid inclusions

Based on the number of constituent phases observed at room temperature, combined with microthermometric behavior, three main types of fluid inclusions were recognized:

Type 1 represents elliptical to well rounded, to irregular aqueous two-phase (liquid + vapor) inclusions. Sizes vary between 10 and 30 μm in the longest dimension. The vapor phase was estimated to occupy 20 to 60 vol. % of the inclusion. Clathrate was observed upon cooling in about 20% of type 1 inclusions, melting at temperatures above 0 °C. These inclusions are classified as type 1a. Aqueous inclusions may form clathrate upon cooling at CO_2 concentrations of approximately 0.85 to 2.2 molal (Collins 1979). The minimum concentration necessary to form an optically detectable liquid CO_2-phase at 10 °C is approximately 2.2 molal for pure water and less for a saline solution (Hedenquist and Henley 1985). Accordingly, a CO_2 content between <0.85 and 2.2 molal is suggested for type 1(1a) inclusions, since a liquid CO_2 phase was not seen.

Type 2 refers to H_2O-CO_2, three-phase inclusions containing an aqueous liquid and CO_2-liquid and vapor phases. The liquid CO_2 always forms a thin film around the gaseous CO_2 and homogenizes to the vapor phase. The combined CO_2 liquid plus vapor were visually estimated to occupy 50 to 90% of the inclusion volume. Type 2 inclusions have equant to rounded shapes and sizes averaging 10 to 40 μm on a side. Total homogenization of type 2 inclusions was either to the liquid or the vapor phase. Consequently, type 2 inclusions are subdivided into subtype 2a which homogenized to the liquid phase and contain from 50 to 60 vol. % CO_2, and sub-type 2b which homogenized to vapor and are characterized by higher than 60% volumetric proportions of the carbonic phase.

Type 3 refers to aqueous three-phase high-salinity inclusions of rare occurrence, and sizes between 10 and 50 μm in the longest dimension. They consist of liquid, vapor and solid phases. The vapor phase was estimated to occupy 20 to 30 vol. % of the inclusion. The solid phases are primarily cubic halite crystals occupying 20 to 40% of the inclusion volume, and infrequently a minute opaque grain, possibly sphalerite.

Setting, distribution and abundances of fluid inclusion types

This study deals only with inclusions fulfilling the requirements to be classified as primary and pseudosecondary

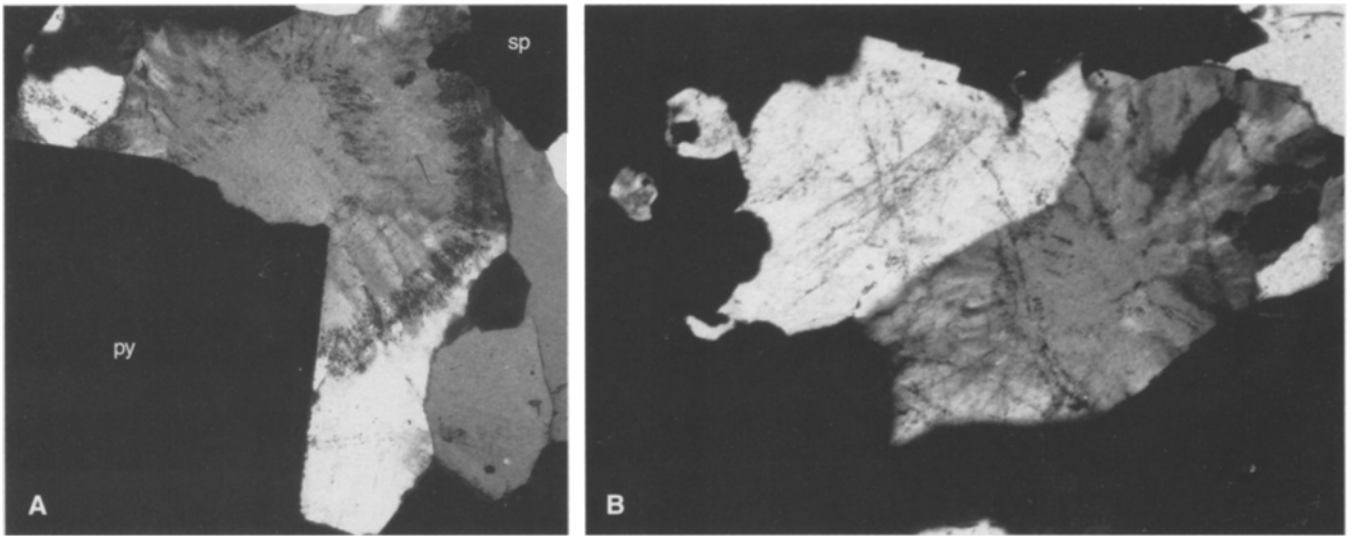

Fig. 3. **A** Euhedral and zoned quartz intergrown with pyrite (*py*) and sphalerite (*sp*) from undeformed ore. Crossed polarizers. 3.6 mm × 3.5 mm. **B** Anhedral quartz intergrown with sphalerite (*black*) from deformed ore. Crossed polarizers, 4.3 mm × 2.3 mm

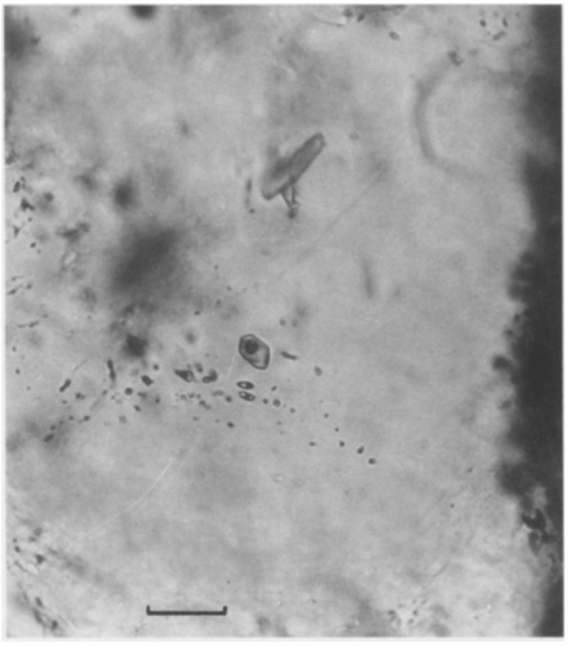

Fig. 4. Type 1 primary inclusions in undeformed quartz intergrown with sulfides (*dark*). Scale bar = 60 μm

(after Roedder 1984), and thus co-genetic with the host crystals.

Primary inclusions occur in the following settings: (1) as irregular three-dimensional clusters characterized by a high density of fluid inclusions outlining, or close to, quartz growth zones (undeformed ore); (2) in 'clear' areas of the host grain characterized by a low density of apparently randomly distributed fluid inclusions (undeformed and deformed ores); and (3) as isolated inclusions occasionally close to quartz-sulfide intergrowth surfaces, or within the number 2 setting (undeformed and deformed ores) (Fig. 4).

Pseudosecondary inclusions occur in subparallel intragranular planar arrays. This inclusion setting is more abundant in deformed quartz. On the basis of the similarity of these inclusions to isolated inclusions of the same type in the same grain, it may be suggested that these inclusions represent fluid entrapment during strain, or fracturing of the host which preceded an interval of quartz precipitation, and not during post-crystallization deformation.

In the undeformed ore type 1 + 1a inclusions are vastly more abundant than type 2b, or 2a, and in some grains may be the only type present. Type 2b inclusions show a higher overall abundance in the deformed ore, where in some grains they may constitute up to 80% by number. Rare, halite-bearing type 3 inclusions have not been observed in the studied deformed samples.

Typically one type of inclusion (type 1 + 1a or 2b) occurs within a cluster or a given planar array. However, a small number of inclusions of the other type (< 10 vol. %) may also be present. Inclusions of all types also occur isolated. Type 3 inclusions are found isolated or in low inclusion density clusters dominated by type 1 inclusions.

Reconnaissance petrographic investigations show that sphalerite crystals contain inclusions identical to those in co-existing quartz, except for the absence of type 3.

Microthermometry results

H_2O-rich fluid inclusion types 1, 1a and 3

Ice, clathrate, and halite melting temperatures, and total homogenization temperatures (*Th*) of inclusion types 1, 1a and 3 are shown in Fig. 5. Corresponding salinities are expressed in terms of equivalent weight percent NaCl, and are estimated in the system H_2O-NaCl from the liquidus temperature of ice (Tm, ICE) (Potter et al. 1978) for type 1 inclusions, the liquidus temperature of halite (Tm, HAL) (Haas 1976) for type 3 inclusions, and in the system H_2O-CO_2-NaCl from the melting temperature of the clathrate (Tm, CLAT) (Collins 1979; Diamond 1992) for type 1a inclusions. Salinity estimations from Tm, CLAT in the case of type 1a inclusions are approximate because no liquid CO_2 was present at the clathrate melting point. The potential error of salinity estimation is not quantitatively known, so no corrections have been made to the data presented here. However, salinity estimates based on clathrate melting points in the absence of liquid CO_2 have been presented as an acceptable approximation of the true salinity of aqueous inclusions with minor amounts of CO_2 detected as clathrates during cooling (So et al. 1993). The presence of KCl, $MgCl_2$, and $CaCl_2$, in addition to NaCl, was indicated in some type 1 inclusions by observed temperatures of first melting of ice between $-25°$ and $-45\,°C$ (data of Borisenko 1977, in Shepherd et al. 1985; Crawford 1981).

Salinities of fluid inclusions from all the examined samples show a large variation ranging between 0.9 and 32.4 equivalent wt. % NaCl. However, excluding the uncommon halite-bearing type 3 inclusions, most salinities fall within the range of 1–18 equivalent wt. % NaCl. Dissolved CO_2 in the aqueous liquid-phase could contribute up to 1.5 °C to the total depression of the ice melting point, reducing the salinity estimates of type 1 inclusions up to 1 equivalent wt. % NaCl (Hedenquist and Henley 1985). It is worth noting that despite the wide scatter, the modal salinities of the H_2O-rich fluids associated with the undeformed ore (3.37 equivalent wt. % NaCl for type 1 inclusions, and 5.77 equivalent wt. % NaCl for type 1a inclusions) are similar to those from the deformed ore (mode at 4.94 equivalent wt. % NaCl).

The majority of the H_2O-rich inclusions homogenize at temperatures between 270° and 350°, except for the halite-bearing ones which have a narrower range of higher *Th* values between 325° and 356 °C (Fig. 5e, f, g, h). All H_2O-rich, liquid-vapor type 1 + 1a inclusions homogenize into the liquid phase and most have calculated densities of 0.61 to 0.84 g/cc when interpreted in the pure H_2O-NaCl system. Densities of type 1a inclusions are approximate because they have been calculated as if CO_2 content were zero. Halite crystals show a consistency in their dissolution temperature and always dissolve before disappearance of the vapor bubble, indicating trapping of an unsaturated solution. The opaque grains show no evidence

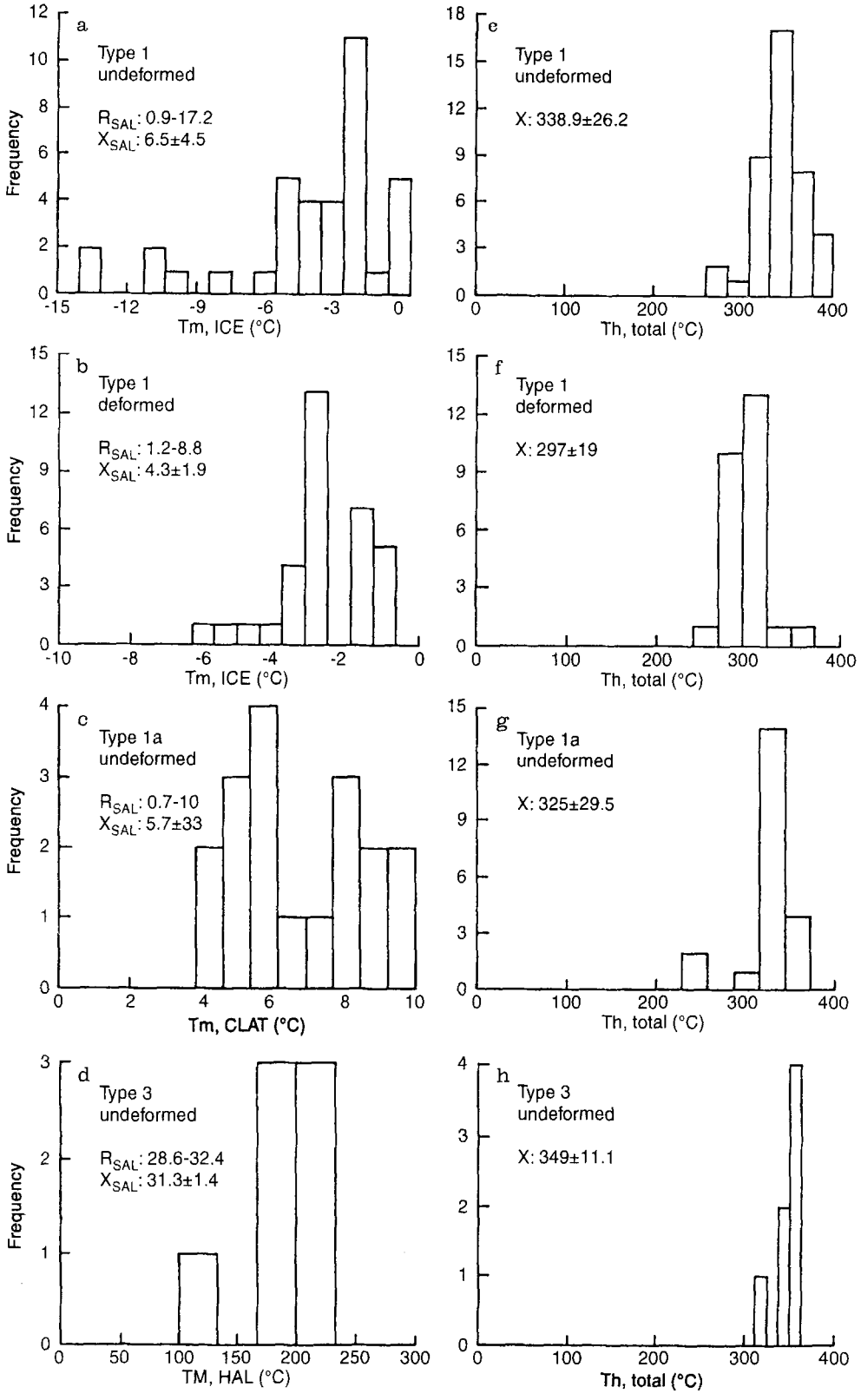

Fig. 5. a, b Histograms of ice melting (Tm, ICE), **c** clathrate melting (Tm, CLAT), **d** halite melting (Tm, HAL), **e, f, g, h** total homogenization temperatures (Th, total) of inclusion types 1, 1a, and 3 from undeformed and deformed ore mineralization (R_{SAL}: range of estimated corresponding salinity, X_{SAL}: average corresponding salinity, X: average, $\pm$: standard deviation)

of melting, even at temperatures higher than the total inclusion homogenization temperatures. Halite-bearing type 3 inclusions homogenize by vapor disappearance, and have calculated densities between 0.95 and 1.01 g/cc. All density calculations were based on the tables of interpolating constants by Potter and Brown (1977).

Figure 6 is a plot of salinity versus total homogenization temperatures in an attempt to depict variation

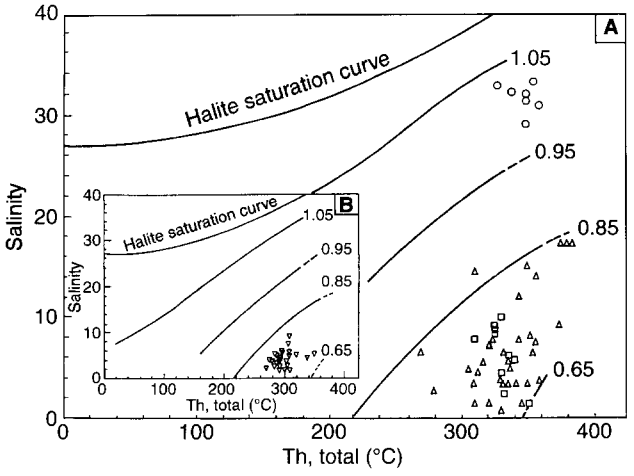

Fig. 6A, B. Salinity (wt. % NaCl equivalent) versus total homogenization temperature (° C) for inclusion types 1(△), 1a(□), and 3(○) in **A** undeformed ore, and inclusion type 1(▽) in **B** deformed ore. NaCl saturation curve (halite + liquid + vapor curve) and selected isodensity curves are also shown (data from Sourirajan and Kennedy 1962; Urusova 1975, and Haas 1976)

patterns and relationships existing among types 1 + 1a and 3 inclusions, as will be discussed later in the study.

Type 2 inclusions

Final melting temperatures of solid CO_2 (Tm, CO_2) in type 2 inclusions are shown in Fig. 7. Type 2 inclusions contain CO_2 as the only non-condensable gas as the corresponding melting temperatures of solid CO_2 (mode, − 56.6 °C) are very close to that of the triple point of CO_2 (Weast 1977).

All type 2 inclusions showed homogenization of the CO_2-phases to the vapor phase, indicating CO_2-phase densities lower than the critical density.

Type 2a inclusions show a very narrow range of CO_2-phase homogenization temperatures from 21.0° to 22.0 °C (mode, 21.3 °C) for the undeformed ore and a wider range between 22.4° and 30.8 °C (mode, 27.4 °C) for the deformed ore (Fig. 8b). These homogenization temperatures indicate CO_2-phase densities of 0.20 ± 0.02 g/cc and 0.26 g/cc, respectively for undeformed and deformed ores (Angus et al. 1976). Salinity estimates, based on the observed clathrate melting temperatures (Fig. 8a), range between 0.41 and 2.4 equivalent wt. % NaCl, with modal values at 1.4 and 1.0 for type 2a fluids associated with undeformed and deformed ore, respectively. Bulk densities of type 2a inclusions range from 0.52 to 0.60 g/cc (mean, 0.56 ± 0.04) and 0.52–0.66 g/cc (mean, 0.60 ± 0.04) for the undeformed and deformed ores, respectively. Type 2a inclusions contain approximately the same calculated amount of CO_2 in both undeformed (7.8–11.5 mol %) and deformed (8.1–14.6 mol %) ores. Type 2a inclusions from the undeformed ore homogenized at temperatures between 331° and 350 °C (mode, 350 °C), whereas total homogenization in the deformed ore occurred between 306° and 350 °C (mode, 350 °C) (Fig. 8c).

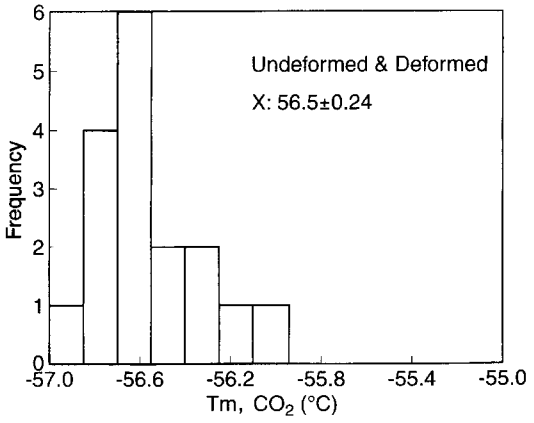

Fig. 7. Histogram of CO_2 melting temperatures of type 2a and 2b inclusions for undeformed and deformed ore (X: average, ±: standard deviation)

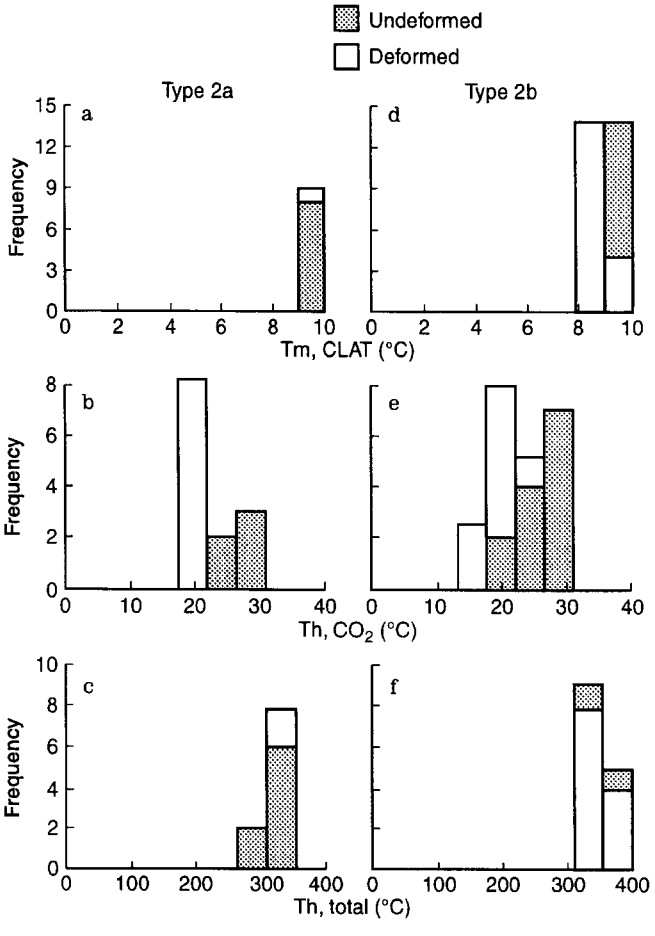

Fig. 8. Histograms of **a, d** clathrate melting (Tm, CLAT), **b, e** CO_2-phase homogenization (Th, CO_2) and **c,f** total homogenization (Th, total) temperatures of inclusion types 2a and 2b for undeformed and deformed ore

The CO_2 phases in type 2b inclusions homogenized between 17.6° and 25.0 °C (mode, 20.9 °C) in undeformed ore, and between 19.2° and 30.4 °C (mode, 26.8 °C) in deformed ore (Fig. 8e) indicating CO_2-phase densities of 0.26 ± 0.04 g/cc and 0.25 ± 0.05 g/cc, respectively.

Table 1. Microthermometry data and properties of inclusion types 2a and 2b

Inclusion	Type	Freezing data (°C) *Tm*, CLAT	Salinity wt. % NaCl	Homogenization data (°C) *Th*, CO_2	*Th*, total	CO_2-content mol %	Density g/cc
2a	U	R:8.9 – 9.4	R:1.0 – 2.4	R:21.0 – 21.9	R:331 – 350	R: 7.8 – 11.5	R:0.52 – 0.60
		X:9.1 ± 0.2	X:1.6 ± 0.7	X:21.4 ± 0.4	X:343 ± 8.0	X: 9.6 ± 1.9	X:0.56 ± 0.04
	D	R:9.0 – 9.8	R:0.41 – 2.0	R:22.4 – 30.8	R:306 – 350	R: 8.1 – 14.6	R:0.52 – 0.66
		X:9.5 ± 0.2	X:1.0 ± 0.6	X:27.1 ± 3.7	X:331 ± 18.0	X:11.4 ± 2.3	X:0.60 ± 0.04
2b	U	R:7.8 – 9.0	R:1.4 – 4.1	R:17.6 – 25.0	R:320 – 382	R:17.9 – 28.5	R:0.35 – 0.43
		X:8.3 ± 0.4	X:2.5 ± 1.2	X:21.2 ± 2.7	X:349 ± 22.5	X:24.2 ± 3.5	X:0.37 ± 0.01
	D	R:8.9 – 9.8	R:1.0 – 2.2	R:19.2 – 30.4	R:312 – 368	R:30.5 – 49.8	R:0.30 – 0.46
		X:9.4 ± 0.3	X:1.5 ± 0.4	X:25.7 ± 3.4	X:345 ± 18.0	X:38.2 ± 6.5	X:0.36 ± 0.05

U: undeformed ore, D: deformed ore, X: mean, ±: standard deviation

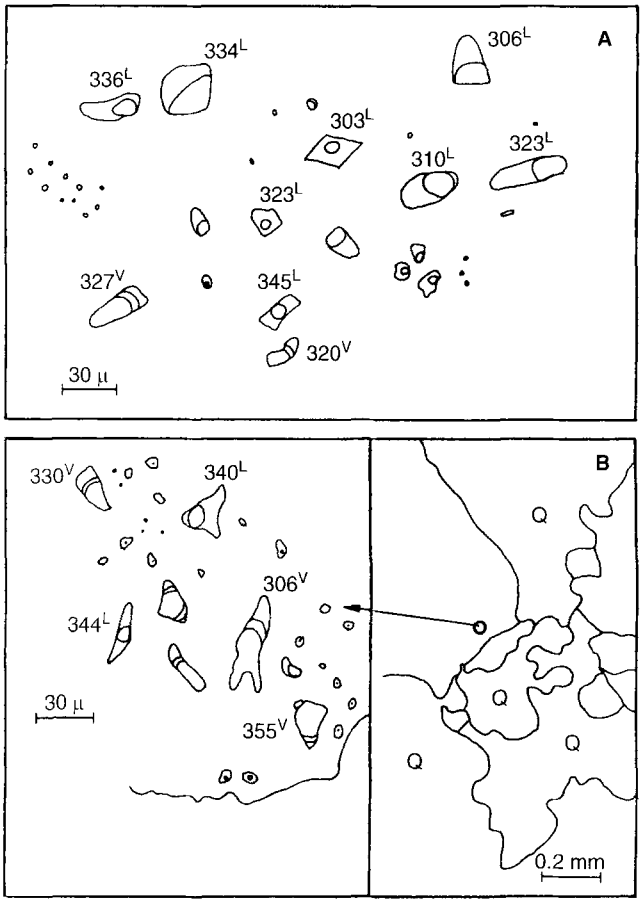

Fig. 9A, B. Sketch showing fluid inclusion types 1 and 2b associations and total homogenization temperature data (°C) (mode of homogenization: *L* into liquid; *V* into vapor). Cluster-like fluid inclusion setting dominated by type 1 inclusions in **A** undeformed quartz. Pseudosecondary planar array of type 2b inclusions (coexisting type 1 inclusions also present) in **B** deformed quartz (Q) with sutured margins

Salinities of type 2b inclusions, estimated on the basis of clathrate melting temperatures (Fig. 8d), range from 1.4 to 4.1, and from 1.0 to 2.2 equivalent wt. % NaCl, in undeformed and deformed ore, respectively. Calculated bulk densities range from 0.35 to 0.43 g/cc (mean, 0.37 ± 0.02) and 0.30 to 0.46 g/cc (mean, 0.36 ± 0.05) for the undeformed and deformed ore, respectively. Calculated molar contents of CO_2 in type 2b inclusions range from 17.9 to 28.5 (mean, 24.2 ± 1.9) (undeformed ore) and 30.5 to 49.8 (mean, 38.2 ± 6.5) (deformed ore). Homogenization temperatures of type 2b inclusions range between 320° and 382 °C (mode, 320 °C) for the undeformed ore, and between 312° and 368 °C (mode, 347 °C) for the deformed ore (Fig. 8f). Microthermometry data and properties of inclusion types 2a and 2b are summarized in Table 1.

Type 2b inclusions coexist with type 1 + 1a inclusions in primary clusters or pseudosecondary planar arrays, in both undeformed and deformed ore (Fig. 9).

Discussion

The fluid inclusion results combined with the observed spatial relationships among the different types of primary and pseudosecondary fluid inclusions indicate trapping of three types of fluids during both undeformed and deformed quartz crystallization. These are: (1) an aqueous high-density moderately saline fluid, low in carbonic content (type 1); (2) an H_2O-CO_2 fluid of low density and low salinity containing varying proportions of H_2O and CO_2 (type 2b); and (3) a H_2O-CO_2 fluid of moderate density and salinity containing relatively constant proportions of CO_2 and H_2O (type 2a). Based on equilibrium textures of quartz and sulfides, coupled with the presence of identical inclusions in coexisting quartz and sphalerite we suggest that inclusions trapped in quartz contain samples of the ore forming fluid. The high-density, high salinity fluid, with no detectable carbonic content, trapped in type 3 inclusions is also indicated to have been an intimate component of the Olympias ore-forming system.

Sphalerite fluid inclusion data are not available at present. However, with the exception of higher inclusion salinities (up to 33 wt. % NaCl equivalent) and homogenization temperatures (about 70 °C), fluid inclusions hosted in undeformed and deformed sphalerite from replacement ores of the Madem Lakos deposit (Fig. 1) are similar to the studied ones from Olympias, both in terms of petrographic, compositional, as well as microthermometric characteristics (Gilg 1993). Taking into account that Olympias and Madem Lakos are considered as the distal, and proximal, phase, respectively, of a single metallogenetic system (Kalogeropoulos et al. 1989) this

similarity may additionally support the concept that the studied fluid inclusions in Olympias contain the ore-forming fluid. Thus, data obtained from quartz-hosted inclusions yield valid information on the physicochemical conditions during development of both the deformed and undeformed ore mineralization at Olympias.

Interpretation of fluid inclusion data

The fluid inclusion data may be interpreted in several ways including: independent co-trapped fluids; trapping of different generations of fluids at different *T-P* conditions; unmixing of a homogeneous fluid.

On the basis of the work of Ramboz et al. (1982) on thermodynamic and chemical principles of phase equilibrium applied to isochoric-isoplethic systems, such as fluid inclusions, several lines of evidence have been provided that inclusion types 1 + 1a and 2b may constitute stable immiscible phases generated by fluid unmixing ("boiling") under fixed T-P conditions.

1. The two types of inclusions are closely related in space, coexisting in the same regions of individual quartz crystals in primary or pseudosecondary assemblages. This in turn may also suggest contemporeneity (e.g. Higgins 1985; Robert and Kelly 1987) (i.e., close relationship in trapping time) of the two inclusion types.
2. The contrasting densities of the two inclusion types lead to total homogenization via opposite phase transition to liquid and vapor phases, respectively. It has already been noted that all type 1 + 1a inclusions homogenize to liquid, whereas surrounding or coexisting type 2b inclusions homogenize to vapor, at overlapping temperatures between 320° and 382 °C (Figs. 5e, f, g; 8c, f; 9A, B).
3. Calculated internal pressures *Ph*, total, at *Th*, total, of inclusion types 1 and 2b only partially overlap (Figs. 10A, B), an apparent contradiction of an important prerequisite of fluid phase equilibria, that the pressures of the immiscible inclusion fluids should reach the same values (trapping pressures) at homogenization. This is shown on Fig. 10, which superimposes *Th*, total and *Ph*, total of inclusion types 1 and 2b for undeformed (Fig. 10A) and deformed (Fig. 10B) ores in *P-T* space. Internal pressures were calculated for type 1 inclusions using the equations given by Haas (1976, Eqs. 3–6), and for type 2b inclusions using the equation of state by Bowers and Helgeson (1983) and the FLINCOR program of Brown (1989).

The partly overlapping areas of Fig. 10 indicate that indeed some type 1 and 2b inclusions were trapped at identical pressures. The discrepancy for the rest of the inclusions may be due to errors in inclusion-phases volume visual estimation or trapping under different *T-P* conditions. However, considering that fluid unmixing is not an isothermal-isobaric process, a significant pressure drop and/or a time delay between entrapment of type 1 and type 2b inclusions in a fluid system undergoing simultaneous unmixing and *P-T* evolution in a tectonically active environment such that of Olympias (Kalogeropoulos et al. 1989), could produce the observed

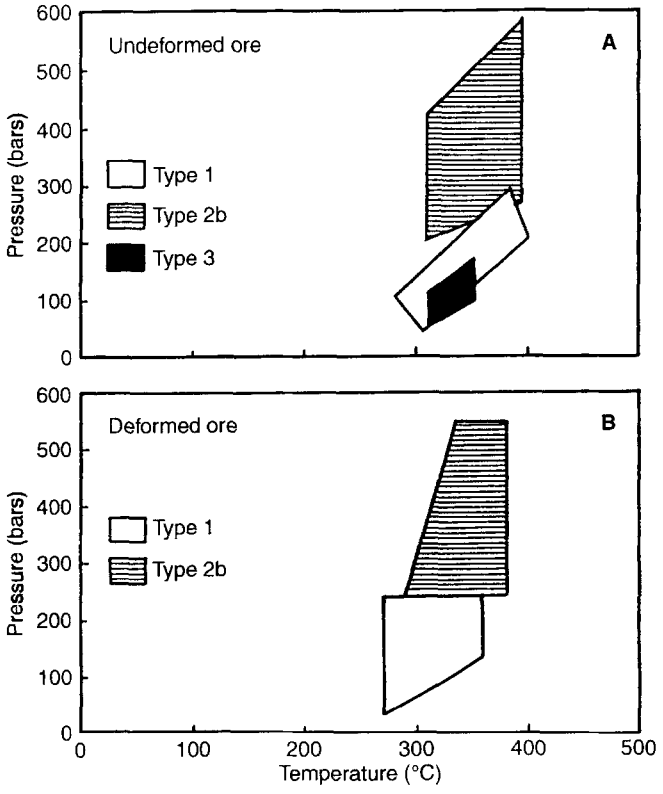

Fig. 10A, B. Comparison of homogenization conditions (Ph, total vs. Th, total) of inclusion types 1, 1a, 2b and 3 for **A** undeformed and **B** deformed ores

pressure difference of 300–400 bar (Ramboz et al. 1982; Diamond 1990). The variation in pressure shown in Fig. 10 (approximately a factor of two to three) may be interpreted geologically to indicate fluctuating pressure conditions between near lithostatic and near hydrostatic, and may constitute the principle cause of immiscibility.
4. Inclusion compositions conform fairly well to chemical equilibrium fractionation at *Th*, total and *Ph*, total. Any chemical species should be distributed between two immiscible fluid phases L(type 1) and V(type 2b) according to:

$K_D, i^{LV} = (Xi^V/Xi^L)_{P,T}$ where

K_D: distribution coefficient and X: composition of species i

The distribution coefficients, calculated from calculated bulk molar compositions of pairs of selected type 1 and type 2b inclusions best representing the equilibrium coexisting immiscible phases (Table 2), display the distribution trend:
$K_D(NaCl) < K_D(H_2O) < K_D(CO_2)$ (Ellis 1979, in Diamond 1990) (Table 3), which may qualitatively be used to show immiscible phases (Diamond 1990). Bulk fluid inclusion compositions were calculated in the system H_2O-CO_2-NaCl assuming that type 1 + 1a inclusions contain CO_2 between < 0.85 and 2.2 molal as evidenced by clathrate formation on freezing, using the FLINCOR program of Brown (1989).

Figure 11 shows the bulk molar compositions of Table 2 plotted on a ternary H_2O-CO_2-NaCl isobaric-isothermal

Table 2. Calculated bulk molar compositions and properties of selected type 1(1a) and 2b inclusions considered to represent immiscible phases in the system H_2O-CO_2-NaCl (see text for discussion)

	Undeformed				Deformed			
	Type 1 (1a)		Type 2b		Type 1 (1a)		Type 2b	
	Pair 1		Pair 2		Pair 1		Pair 2	
H_2O	90.4 – 92.6	93.4 – 95.6	76.20	80.20	94.8 – 97	93.6 – 95.8	68.80	56.00
CO_2	1.4 to	3.6	23.30	18.80	1.4 to	3.6	31.00	43.00
NaCl	6.00	3.00	0.50	1.00	1.60	2.80	0.20	0.40
wt. % NaCl equivalent	17.20	9.20	2.00	3.90	4.95	8.81	1.20	1.80
Density (g/cm^3)	0.79	0.69	0.35	0.47	0.67	0.79	0.32	0.43
Molar volume (cm^3)	25.70	27.70	69.10	48.80	27.50	23.9	81.80	68.40

Table 3. Chemical distribution coefficients (K_D). calculated from data in Table 2 showing the relative trend $K_D(NaCl) < K_D(H_2O) < K_D(CO_2)$ (see text for discussion)

Inclusion pair	Undeformed		Deformed	
	1	2	1	2
K_DNaCl	0.08	0.33	0.12	0.14
$K_D H_2O$	0.82 – 0.84	0.84 – 0.86	0.70 – 0.72	0.58 – 0.60
$K_D CO_2$	6.50 – 16.70	5.30 – 13.40	8.60 – 22.1	11.90 – 30.70

K_D. $i^{L,V} = (Xi^V/Xi^L)_{P,T}$ where:
K_D: distribution coefficient and X: composition of species i

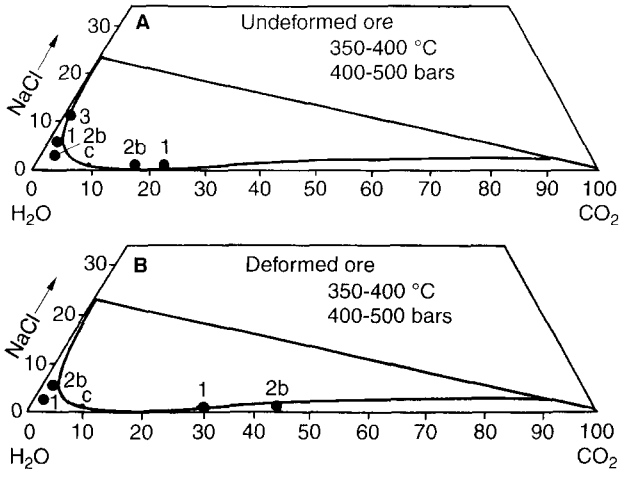

Fig. 11A, B. Calculated bulk molar composition ternary (H_2O-CO_2-NaCl) plot of pairs (1, 2) of coexisting type 1 and 2b inclusions for **A** undeformed and **B** deformed ore. The experimental limits of immiscibility in the system H_2O-CO_2-NaCl at temperatures of 350–400 °C, and pressure of 400–500 bar are shown for comparison (Gehrig 1980). The *dot* along the immiscibility boundary *c* indicates the position of the consolute point at which "liquid" (type 1) and "vapor" (type 2b) become indistinguishable. –3 in **A** designates the area where calculated bulk molar compositions of type 3 inclusions (see text) are plotted

diagram exhibiting the limits of immiscibility at temperatures of 350°–400 °C and pressures of 400–500 bar based on experimental data of Gehrig (1980). Bulk compositions compare favorably with the experimental data, thus strongly indicating the occurrence of immiscibility.

Based on the combination of all the previous lines of evidence, we suggest that higher-temperature type 1 and type 2b inclusions constitute stable immiscible phases, generated by unmixing of a single homogeneous saline aqueous CO_2-bearing parent fluid as its P-T evolution path crossed a solvus surface at temperatures of 350° to 400 °C and pressures of 400–500 bar. Since in different samples type 2a inclusions all contain the same amount of CO_2 (see Microthermometry results), it may be suggested that these inclusions represent the parent fluid before unmixing (Robert and Kelly 1987).

A fluid pH increase due to volatile species (CO_2) separation during unmixing may be suggested as an effective mechanism of deposition of ore-sulfides (Hedenquist and Henley 1985).

Since inclusion types 1 + 1a and 2b may well be unmixing products, homogenization T-P conditions are, in principle, equal to trapping T-P conditions (Pichavant et al. 1982; Ramboz et al. 1982). Therefore we suggest that the Olympias ores were deposited from a fluid undergoing unmixing at temperatures of 350 ± 30 °C and fluctuating pressures of 100 to 500 bar (Fig. 10). The presence of type 2a inclusions indicates that during deposition the P-T

conditions were such that the fluid was above the two-phase region and that the parent homogeneous CO_2-bearing fluid was trapped (Robert and Kelly 1987). The overall similarity in fluid composition, and P-T formation conditions, of the deformed and undeformed ores supports a conclusion that both ore varieties are integral parts of the same metallogenetic system.

Salinity versus temperature trends

Two features shown in Fig. 6 demand explanation:

1. Type 1 inclusions display a wide range of salinities from 0.9 to 17.2 wt. % NaCl equivalent.
2. A complete gap exists between the salinities of type 1 inclusions, and those of type 3 inclusions (undeformed ore) which cluster within a narrow range of 28.6–32.5 wt. % NaCl equivalent.

The salinity range of type 1 inclusions is probably the result of a complex overprinting between a near vertical salinity enrichment trend with decreasing temperature, caused by unmixing, due to decreasing volatile (CO_2) content during adiabatic cooling (Drummond and Ohmoto 1985), and a positive correlation trend between decreasing salinity and temperature due to mixing (dilution) of the high-temperature moderate-salinity unmixed fluid with cooler low-salinity meteoric waters (Reed and Spycher 1985; Shepherd et al. 1985). The involvement of meteoric waters in the Olympias system is supported by salinities well below that of seawater (3.2 wt. % NaCl equivalent), final melting temperatures very close to that of pure water (0.0 °C) (Fig. 5a, b), and oxygen isotope ratios (Kalogeropoulos and Kilias 1989).

If the gap between the salinity trends of inclusion types 1 and 3 (from 17.2 to 28.6 wt. % NaCl equivalent) is real, unmixing or mixing as major mechanisms for generation of the high-salinity type 3 inclusions may be precluded, because in both cases fluid inclusions with the missing salinities should have been present. In this case, a probable early high-P and T, high-salinity fluid recorded in type 3 inclusions should be invoked. This fluid could be the result of the following mechanism: boiling (phase separation) of an original aqueous fluid derived from a crystallizing magma, either upon release from the magma (Bodnar et al. 1985), or due to a pressure drop (volume increase caused by fault movements, after Roedder 1984, p. 270) along its cooling path. If this phase separation, into a high salinity liquid (type 3 inclusions) and a low salinity vapor occurred at depth below the site of ore deposition, the vapor phase might not have been trapped in ore assemblages (Shelton 1983). In this context, the fluid trapped in type 3 inclusions should have remained at higher pressures than the one which unmixed to generate inclusion types 1 + 1a and 2b. It should be noted here that the composition and the maximum entrapment temperatures of type 1 (and 2b) inclusions are consistent with derivation from a cooled original homogeneous aqueous fluid derived from a crystallizing magma (Burnham 1979). This fluid could have been later transformed by phase unmixing at the trapping conditions (as shown), and also mixing with cooler meteoric waters. A magmatic origin of the Olympias fluids is supported by oxygen isotope evidence (Kalogeropoulos and Kilias 1989). This latter magmatic fluid ought to have been generated at P (lithostatic)-T conditions within the one-phase field of the H_2O-CO_2-NaCl system to avoid instant boiling, and cooled without any excessive pressure drop to reach the trapping conditions unchanged.

However, the salinity gap of Fig. 6 may be an artifact due to metastability in the region near halite saturation (Roedder 1984, p. 447–448). Consequently, the unmixing process which produced the inclusion types 1 + 1a and 2b may have almost isothermally driven the residual liquid toward halite saturation, as shown in Fig. 6, during occasional "opening" of the system and concomitant vapor (CO_2) loss, to generate the fluids recorded in type 3 inclusions. Vapor loss as a mechanism for fluid saturation in salt components has been indicated by Trommsdorf and Skippen (1986) in metasomatic phenomena in the Swiss Alps. Under the constraint of the salinity gap, the latter interpretation is supported by overlapping calculated Ph, total of inclusion types 1 and 3 (Fig. 10A), and the satisfactory fit of calculated type 3 bulk molar compositions to chemical equilibrium fractionation at the conditions inferred for unmixing (Fig. 11A), allowing for the possibility that type 3 inclusions formed undetected clathrates (content max. 2.2 molal CO_2). Calculated bulk molar compositions of type 3 inclusions may range: H_2O: 85.6 to 83.8; CO_2: 3.4 to 3.3; NaCl: 11 to 12.9 for salinities of 28.6 to 32.5% NaCl equivalent (CO_2 values are maximum).

Comparison with other Pb-Zn deposits

Figure 12 shows plots of fluid inclusion salinity (wt. % NaCl equivalent) versus total homogenization temperature (°C) data from Olympias in comparison to skarn-type Pb-Zn replacement ores (Naica, Providencia, Groundhog, Washington Camp, Hidalgo, Uchucchacua), carbonate-replacement, skarn-free Pb-Zn(Ag) ores (Taebaek, Bluebell), epithermal polymetallic Ag-Pb-Zn (Au) ores (Creede, Finlandia, Sunnyside), and polymetallic Ag-Pb-Zn(Au) systems, either spatially related to granitic plutons (Keno Hill), or hosted by "granitic" batholiths (Beaverdell) (for references see Fig. 12 caption). Similarity of the Olympias fluids in terms of T-salinity gradients with the "granite"-related ores, the lower-T distal parts of skarn systems, and the skarn-free carbonate-replacement and epithermal environments, is shown. Salinity-T gradients in most of these deposits have been ascribed to mixing of high-temperature saline fluids of either possible or demonstrable magmatic origin, with low-temperature, low-salinity meteoric waters, and/or fluid boiling. Meteoric waters have been recognized as a major source of ore fluids for the epithermal deposits (Creede, Finlandia, Sunnyside). Boiling and fluid immiscibility, and/or mixing, have been recognized, along with fluid-host interactions, as important ore-deposition mechanisms, in these deposits.

The estimated formation-pressure conditions of the Olympias deposit are similar to those recorded in the lower pressure part of the "granite"-related Keno Hill, Canada (P: 468–675 bar), the lower-temperature distal

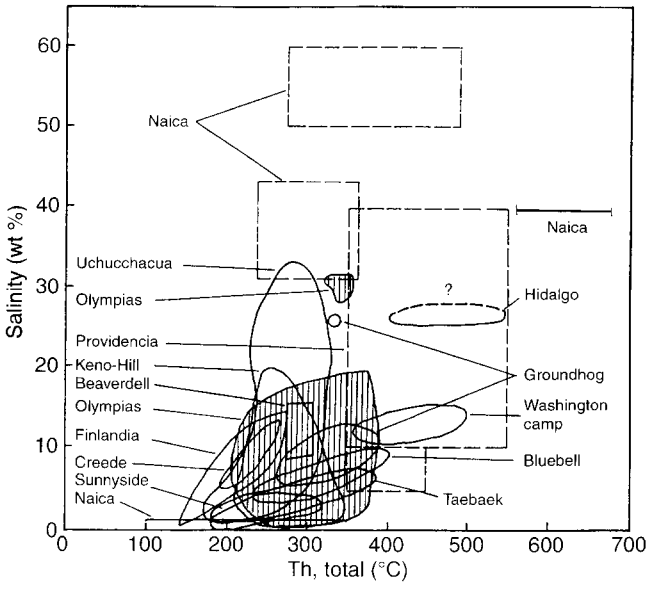

Fig. 12. Comparison of fluid inclusion salinity (wt. % NaCl equivalent) versus total homogenization temperatures (°C) plots of *Pb-Zn skarn-type deposits* Naica, Mexico (Erwood et al. 1979 and data in Megaw et al. 1988), Providencia, Mexico (Sawkins 1964 and data in Megaw et al. 1988), Groundhog, USA (Meinert 1987), Washington Camp, USA (Surles 1978 in Kwak 1986), Hidalgo, Mexico (Simone 1951 in Kwak 1986), Uchucchacua, Peru (Bussel et al. 1990), *carbonate-replacement skarn-free Pb-Zn (Ag) deposits* (Taebaek, Korea (So et al. 1993), Bluebell, Canada (Ohmoto and Rye 1970), *epithermal polymetallic Ag-Pb-Zn (Au) deposit* (Creede, USA (Woods et al. 1982 in Hedenquist and Henley 1985), Finlandia, Peru (Kamilli and Ohmoto 1977, Sunnyside, USA (Casadeval and Ohmoto 1977), and *polymetallic Ag-Pb-Zn(Au) systems associated with "granitic" intrusions* (Keno Hill, Canada (Lynch et al. 1990) Beaverdell, Canada (Godwin et al. 1986) with the *Olympias deposit*

parts of skarn systems as in Providencia, Mexico (*P*: 300 bar), Naica, Mexico (*P*: 300 bar), and Groundhog, N. Mexico (*P*: 155–175 bar); and also the limestone replacement Bluebell, Canada (*P*: 300–800 bar), and Taebaek, Korea (*P*: 210–420 bar), and the epithermal Sunnyside, USA (*P*: 110–220 bar). The CO_2 content of the Olympias inclusions is high enough to form a distinct liquid CO_2 phase. With the exception of Keno Hill, Canada, the formation of liquid CO_2 was not noted in any of the fluid inclusion studies included in this comparison. In other deposits, the presence of CO_2 in the inclusions has been either indirectly recognized by clathrate formation (Taebaek, Bluebell), crushing tests (Creede), or assumed as the gas which was condensed by liquid N_2 (Finlandia, Sunnyside). The occurrence of unmixing at Olympias may have been promoted by the relatively higher CO_2 contents of the mineralizing fluids compared to other carbonate-hosted replacement deposits such as Taebaek, Korea and Bluebell, Canada, formed at comparable *P-T* conditions, where no evidence of immiscibility has been reported.

Conclusions

Fluid inclusion systematics in both undeformed and deformed mineralization of the carbonate-hosted Olympias deposit may be explained by trapping during unmixing of an aqueous, high-temperature, CO_2-bearing fluid of low salinity. Fluid unmixing, and concomitant ore-mineralization, took place at temperatures of 350 ± 30 °C and fluctuating pressures of less than 500 bar. Observed fluid salinity variability may be due to solute enrichment of the residual liquid, as a result of volatile separation during phase unmixing, coupled by the imprint of diluting low-salinity meteoric waters. Pressure and temperature formation conditions of the deformed ore, combined with its mineralizing-fluid similarity to undeformed ore, precludes a premetamorphic syngenetic origin. Comparative data show a similarity of the Olympias fluids in terms of salinity-temperature gradients with other Pb-Zn mineralizing fluid gradients formed in "granite"-related, low-*T* distal-skarn, skarn-free carbonate-replacement, and epithermal environments.

Acknowledgements. The constructive review of Dr. Kevin Shelton greatly improved the content of this manuscript.

References

Angus, S., Armstrong, B., De Reuc, K.M. (1976) International thermodynamic tables of fluid state 3: carbon dioxide. Pergamon Press, Oxford, 386 pp

Bodnar, R.J., Burnham, C.W., Sterner, S.M. (1985) Synthetic fluid inclusions in natural quartz. III. Determination of phase equilibrium in the system H_2O-NaCl to 1000 °C and 1500 bar. Geochim. Cosmochim. Acta 49:1861–1873

Borisenko, A.S. (1977) Study of the salt composition of solutions in gas-liquid inclusions in minerals by the cryometric method. Soviet. Geol. Geophys 18:11 19

Bowers, T.S., Helgeson, H.C. (1983) Calculation of the thermodynamic and geochemical consequences of non ideal mixing in the system H_2O-CO_2-NaCl on phase relations in geologic systems: equation of state for H_2O-CO_2-NaCl fluids at high pressures and temperatures. Geochim. Cosmochim. Acta 47:1247–1275

Brown, P.E. (1989) FLINCOR: a microcomputer program for the reduction and investigation of fluid inclusion data. Am. Mineral. 74:1390–1393

Burnham, C.W. (1979) Magmas and hydrothermal fluids. In: Barnes, H.L. (ed.) Geochemistry of hydrothermal ore deposits, 2nd ed. Wiley and Sons, New York, pp. 71–136

Bussell, M.A., Alpers, C.N., Petersen, U., Shepherd, T.J., Bermudez, C., Baxter, A.N. (1990) The Ag-Mn-Pb-Zn vein, replacement and skarn deposits of Uchucchacua, Peru: studies of structure, mineralogy, metal zoning, Sr isotopes and fluid inclusions. Econ. Geol. 85:1348–1383

Casadevall, T., Ohmoto, H. (1977) Sunnyside mine, Eureka mining district, San Juan, Colorado: geochemistry of gold and base metal ore deposition in a volcanic environment. Econ. Geol. 72:1285–1320

Collins, P.L.F. (1979) Gas hydrates in CO_2-bearing fluid inclusions and the use of freezing data for estimation of salinity. Econ. Geol. 74:1435–1444

Crawford, M.L. (1981) Phase equilibria in aqueous fluid inclusions. Mineralog. Assoc. Canada Short Course Handbook 6:75–100

Diamond, L.W. (1990) Fluid inclusion evidence for P-V-T-X evolution of hydrothermal solutions in late-Alpine gold-quartz veins at Brusson, Val D' Ayas, NW Italian Alps. Am. J. Sci. 290:912–958

Diamond, L.W. (1992) Stability of CO_2 clathrate hydrate + CO_2 liquid + CO_2 vapor + aqueous KCl-NaCl solutions: experimental determination and application to salinity estimates of fluid inclusions. Geochim. Cosmochim. Acta 56:273–280

Drummond, S.E., Ohmoto H. (1985) Chemical evolution and mineral deposition in boiling hydrothermal systems. Econ. Geol. 80:126–147

Ellis, A.J. (1979) Explored geothermal systems. In: Barnes H.L. (ed.) Geochemistry of hydrothermal ore deposits, 2nd edn. Springer, New York, pp. 632–683

Erwood, R.J., Kesler, S.E., Cloke, P.L. (1979) Compositionally distinct, saline hydrothermal solutions, Naica mine, Chihuaua, Mexico. Econ. Geol. 74:95–108

Gehrig, M. (1980) Phasengleichgewichte und pVT-Daten ternaerer mischungen aus Wasser, Kohlendioxid und Natriumchlorid bis 3 kbar und 550 C. Hochschulsammlung Naturwissenschaft, Chemie Band 1, Hochschulverlag, Freiburg, 109 pp

Gilg, H.A., Frei, R., Kalogeropoulos, S.I., Nicolaou, M. (1992) Metamorphism and polygenesis of the Madem Lakos polymetallic sulfide deposit, Greece-a discussion. Econ. Geol. 87:1184–1193

Gilg, H.A. (1993) Geochronology (K-Ar), fluid inclusion, and stable isotope (C,H,O) studies of skarn, porphyry copper, and carbonate-hosted Pb-Zn (Au, Ag) replacement deposits in the Kassandra mining district. Unpub. Ph.D. Thesis, ETH Zurich, 153 pp

Gilg, H.A., Frei, R. (1994) Chronology of magmatism and mineralization in the Kassandra mining area, Greece. The potentials and limitations of dating hydrothermal illites. Geochim. Cosmochim. Acta 58:2107–2122

Godwin C.I., Watson, P.H., Shen, K. (1986) Genesis of the Lass vein system, Beaverdell silver camp, south-central British Columbia. Can. J. Earth Sci. 23:1615–1626

Haas, J.L., Jr. (1976) Physical properties of the coexisting phases and thermochemical properties of the H_2O component in boiling NaCl solutions. US Geol. Survey Bull., 1421-A, 73 pp

Hedenquist, J.W., Henley, R.W. (1985) The importance of CO_2 freezing point measurements of fluid inclusions: evidence for geothermal systems and implications for epithermal ore deposition. Econ. Geol. 80:1379–1406

Higgins, N.C. (1985) Wolframite deposition in a hydrothermal vein system: the Grey River tungsten prospect, Newfoundland, Canada. Econ. Geol. 80:1297–1327

Kalogeropoulos, S.I., Bitzios, D., Eliopoulos, D., Veranis, N. (1987) Geological, mineralogical and geochemical study of the Olympias type Pb-Zn (Au, Ag) sulfide ore deposit, E. Chalkidiki, N. Greece. Contribution to its metallogeny. Mineral Dep. Res. 19, I.G.M.E., 36 pp

Kalogeropoulos, S.I., Kilias, S.P. (1989) Oxygen (^{18}O) and carbon (^{13}C) isotopic changes in carbonate rocks and minerals in relation to the Olympias Pb-Zn (Au, Ag) sulfide mineralization, E, Chalkidiki, N. Greece. Contribuion to metallogeny and exploration. Geol. Soc. Greece Bull. 23/2:261–269 (in Greek with English Abstract)

Kalogeropoulos, S.I., Kilias, S.P., Bitzios, D.C., Nicolaou, M., Both, R.A. (1989) Genesis of the Olympias carbonate-hosted Pb-Zn (Au, Ag) sulfide ore deposit, Eastern Chalkidiki Peninsula, N. Greece. Econ. Geol. 84:1210–1234

Kamilli, R.J., Ohmoto, H. (1977) Paragenesis, zoning, fluid inclusion and isotopic studies of the Finlandia vein, Colqui district, central Peru. Econ. Geol. 72:950–982

Kilias, S.P., Kalogeropoulos, S.I. (1989) Physicochemical conditions during sulfide formation of the Olympias carbonate- hosted Pb-Zn (Au, Ag) sulfide ore deposit, eastern Chalkidiki Peninsula, N. Greece: evidence from fluid inclusions and arsenopyrite geothermometry. Geol. Soc. Greece Bull. 23/2:271–282 (in Greek with English Abstract)

Kockel, F., Molat, H., Walther, H. (1977) Erlanterung en zur geologiscen Karte der Chalkidiki und angrenzender Gebiete 1:100000, Nordgriechenland. Bundesamt. Geowiss. Rohst., Hannover, 119 pp

Kwak, T.A.P. (1986) Fluid inclusions in skarns (carbonate replacement deposits). J. Metam. Geol. 4:363–384

Lynch, J.V.G., Longstaffe, F.J., Nesbitt, B.E. (1990) Stable isotopic and fluid inclusion indications of large-scale hydrothermal paleoflow, boiling, and fluid mixing in the Keno Hill Ag-Pb-Zn district, Yukon Territory, Canada. Geochim. Cosmochim. Acta. 54:1045–1059

Mantzos, L.A. (1989) Geology and lithogeochemistry of the Olympias carbonate-hosted Pb-Zn sulfide deposit, Chalkidiki, Greece. Unpub. Ph.D. Thesis, Imperial College, University of London, 404 pp

Megaw, P.K.M., Ruiz, J., Titley, S.R. (1988) High-temperature, carbonate-hosted Ag-Pb-Zn (Cu) deposits of Northern Mexico. Econ. Geol. 83:1856–1885

Meinert, L.D. (1987) Skarn zonation and fluid evolution in the Groundhog mine, Central mining district, New Mexico. Econ. Geol. 82:523–545

Nebel, M.L., Hutchinson, R.W., Zartman, R.E. (1991) Metamorphism and polygenesis of the Madem Lakos polymetallic sulfide deposit, Chalkidiki, Greece. Econ. Geol. 86:81–105

Nebel, M.L., Hutchinson, R.W., Zartman, R.E. (1992) Metamorphism and polygenesis of the Madem Lakos polymetallic sulfide deposit, Chalkidiki, Greece – a reply. Econ. Geol. 87:1187–1190

Nicolaou, M., Kokonis, I. (1980) Geology and development of Olympias mine, Eastern Chalkidiki, Macedonia, Greece. In: Jones M.J. (ed.) Complex sulfide ores, London Inst. Mining Metallurgy, pp. 260–270

Ohmoto, H., Rye, R.O. (1970) The Bluebell mine, British Columbia, mineralogy, paragenesis, fluid inclusions, and the isotopes of hydrogen, oxygen, and carbon. Econ. Geol. 65:417–437

Pichavant, M., Ramboz, C., Weisbrod, A. (1982) Fluid immiscibility in natural processes: use and misuse of fluid inclusion data. I. Phase equilibria analysis – a theoretical and geometrical approach. Chem. Geol. 37:1–27

Potter, R.W., II., Brown, D.L. (1977) The volumetric properties of aqueous sodium chloride solutions from 0 °C to 500 °C at pressures up to 2000 bar based on a regression of available data in the literature. US Geol. Survey Bull. 1421-C, 36 pp

Potter, R.W., II., Clynne, M.A., Brown, D.L. (1978) Freezing point depression of aqueous sodium chloride solutions. Econ. Geol. 73:284–285

Poty, B., Leroy, J., Jachimowicz, L. (1976) Un nouvel appareil pour la mesure de temperatures sous le microscope: I: installation de microthermometrie Chaixmeca. Bull. Mineral. 99: 182–186

Ramboz, C., Pichavant, M., Weisbrod, A. (1982) Fluid immiscibility in natural processes: use and misuse of fluid inclusion data in terms of immiscibility. Chem. Geol. 37:29–48

Reed, M.H., Spycher, N.F. (1985) Boiling, cooling and oxidation in epithermal systems: A numerical modeling approach. In: Berger, B.R., Bethke, P.M. (eds.) Geology and geochemistry of epithermal systems, Reviews in Economic Geology 2:249–272

Robert, F., Kelly, W.C. (1987) Ore-forming fluids in Archean gold-bearing quartz veins at the Sigma mine, Abitibi greenstone belt, Quebec, Canada. Econ. Geol. 82:1464–1482

Roedder, E. (1984) Fluid inclusions. Mineral. Soc. Am., Reviews in Mineralogy 12:644 pp

Sawkins, F.J. (1964) Lead-zinc ore deposition in the light of fluid inclusions, Providencia mine, Zacatecas, Mexico. Econ. Geol. 59:883–919

Shelton, K.L. (1983) Composition and origin of ore-forming fluids in a carbonate-hosted porphyry copper and skarn deposit: a fluid inclusion and stable isotope study of Mines Gaspe, Quebec. Econ. Geol. 78:387–421

Shepherd, T.J., Rankin, A.H., Alderton, D.H.M. (1985) A practical guide to fluid inclusion studies. In: Shepherd, T.J., Rankin, A.H., Alderton, D.H.M. (eds.). Blackie, New York

Simone, I.S. (1951) Geology and ore deposits of the Zimapan mining district, Mexico. Unpub. Ph.D. Thesis, Stanford University, 237 pp

So, C., Yun, S., Koh, Y. (1993) Mineralogic, fluid inclusion, and stable isotope evidence for the genesis of carbonate-hosted Pb-Zn(-Ag) orebodies of the Taebaek deposit, Republic of Korea. Econ. Geol. 88:855–872

Sourirajan, S., Kennedy, G.S. (1962) The system H_2O-NaCl at elevated temperatures and pressures. Am. J. Sci. 260:115–141

Surles, T.L. (1978) Chemical and thermal variations accompanying formation of garnet skarns near Patogonia, Arizona. Unpub. M.Sc. Thesis, University of Arizona, 54 pp

Trommsdorf, V., Skippen, G. (1986) Vapor loss ("Boiling") as a mechanism for fluid evolution in metamorphic rocks. Contrib. Mineral. Petrol. 94:317–322

Urusova, M.A. (1975) Phase equilibria and thermodynamic characteristics of solutions in the system H_2O-NaCl and NaOH-H_2O at 350–550 °C. Geochem. Int. 11:944–950

Woods, T.L., Roedder, E., Bethke, P.M. (1982) Fluid inclusion data on samples from Creede, Colorado, in relation to mineral paragenesis. US Geol. Survey Open-File Rept. 82–313, 77 pp

Weast, R.C. (1977) CRC Handbook of chemistry and physics. CRC Press, Cleveland, Ohio